CHAPTER SIXTEEN

Directed Actin Assembly and Motility

Rajaa Boujemaa-Paterski[1], Rémi Galland, Cristian Suarez, Christophe Guérin, Manuel Théry, Laurent Blanchoin

Institut de Recherches en Technologies et Sciences pour le Vivant, iRTSV, Laboratoire de Physiologie Cellulaire et Végétale, CNRS/CEA/INRA/UJF, Grenoble, France
[1]Corresponding author: e-mail address: rajaa.paterski@cea.fr

Contents

Abstract

The actin cytoskeleton is a key component of the cellular architecture. However, understanding actin organization and dynamics *in vivo* is a complex challenge. Reconstitution of actin structures *in vitro*, in simplified media, allows one to pinpoint the cellular biochemical components and their molecular interactions underlying the architecture and dynamics of the actin network. Previously, little was known about the extent to which geometrical constraints influence the dynamic ultrastructure of these networks. Therefore, in order to study the balance between biochemical and geometrical control of complex actin organization, we used the innovative methodologies of UV and laser patterning to design a wide repertoire of nucleation geometries from which we assembled branched actin networks. Using these methods, we were able to reconstitute complex actin network organizations, closely related to cellular architecture, to precisely direct and control their 3D connections. This methodology mimics the actin networks encountered in cells and can serve in the fabrication of innovative bioinspired systems.

Methods in Enzymology, Volume 540
ISSN 0076-6879
http://dx.doi.org/10.1016/B978-0-12-397924-7.00016-9

1. INTRODUCTION

The actin cytoskeleton is critical for cellular integrity and is involved in many fundamental phenomena ranging from cell morphogenesis to cell division and motility. It is composed of extremely complex arrays of specialized and dynamic structures that overlap and interconnect continuously overtime. During the past decades, tremendous efforts have been focused on understanding the molecular mechanisms underlying actin cytoskeleton dynamics and elucidating physical properties of actin organization (Blanchoin, Boujemaa-Paterski, Sykes, & Plastino, 2014; Fletcher & Mullins, 2010; Mogilner & Zhu, 2012; Pollard, Blanchoin, & Mullins, 2000). In particular, reconstituted biomimetic systems, able to mimic motility of bacteria, viruses, or vesicles in cytoplasmic extracts or in a purified media, opened up a generation of assays, which significantly deepened our understanding of the essential biochemical components necessary for actin-based force generation (Bernheim-Groswasser, Wiesner, Golsteyn, Carlier, & Sykes, 2002; Cameron, Footer, Van Oudenaarden, & Theriot, 1999; Frishknecht et al., 1999; Giardini, Fletcher, & Theriot, 2003; Loisel, Boujemaa, Pantaloni, & Carlier, 1999; Theriot, Rosenblatt, Portnoy, Goldschmidt-Clermont, & Mitchison, 1994; Vignjevic et al., 2003). However, most of these assays were based on a steady-state balance between unpolymerized and polymerized actin and allowed a macroscopic description of actin assembly and dynamics around the motile particle (Loisel et al., 1999; Romero et al., 2004). Recently, a new generation of motility assays made of a large pool of unpolymerized actin, similar to physiological conditions, unveiled the link between molecular mechanisms of assembly and macroscopic properties of actin branched organization (Achard et al., 2010; Akin & Mullins, 2008; Dayel et al., 2009; Kawska et al., 2012; Reymann et al., 2011). However, how geometrical boundaries influence network dynamics and architecture remains poorly understood.

The innovative technology of micropatterning paves the way for investigations aimed at deciphering the balance existing between geometrical and biochemical constraints in controlling the architectural organization and dynamics of actin. Indeed, extremely simplified media allowing directed growth of actin networks from functionalized patterned geometries has demonstrated that actins self-organize into specific architectures with respect to both biochemical and geometrical constraints (Reymann et al., 2010, 2012). Interestingly, these methods revealed that the network's architecture

governs its own selective interaction with regulatory proteins (Reymann et al., 2010, 2012). Specifically, these studies have demonstrated that, under specific geometrical constraints, actin filaments can self-assemble into parallel, filopodia-like structures, entangled networks, or an antiparallel organization that becomes contractile in the presence of molecular motors. With further improvement in micropatterning and by increasing the number of regulatory proteins used in the assays, it became possible to reconstitute the assembly of complex branched actin architectures similar to those assembled at the leading edge of motile cells or to control and direct 3D actin assembly (Galland et al., 2013). Here, we will first describe how to reconstitute actin-based bead motility in physiologically relevant medium made of a large pool of actin monomers. Second, we will describe how to design UV-micropatterned motifs that can drive the assembly of geometrically controlled actin networks. Finally, we will detail the laser-assisted micropatterning method that allows the reconstitution of directed 3D connections linking adjacent cross-linked actin networks.

2. RECONSTITUTION OF ACTIN-BASED MOTILITY IN A G-ACTIN-BUFFERED MEDIUM

In the following section, we present how to reconstitute motility in a G-actin-buffered medium. Capping protein (CP) is mandatory for symmetry breaking and motility (Iwasa & Mullins, 2007; Loisel et al., 1999). However, at the concentration used in motility assays (Achard et al., 2010; Akin & Mullins, 2008; Loisel et al., 1999; Reymann et al., 2011), which is usually 20–50 n*M*, CP activates spontaneous nucleation of actin monomers in solution. Indeed, CP nucleates actin by stabilizing the nuclei at their barbed end leaving them free to elongate from their pointed end (Schafer, Jennings, & Cooper, 1996). Therefore, in order to confine actin nucleation and elongation to the functionalized bead surface and avoid CP-mediated nucleation in the medium, we saturate actin monomers with profilin rather using free actin monomers; profilin–actin complexes are unable to spontaneously nucleate or undergo pointed-end elongation. Interestingly, profilin–actin complexes are capable of elongating from the barbed ends via nucleation by the Arp2/3 complex at the bead surface (Pantaloni and Carlier, 1993; Fig. 16.1).

2.1. Particles functionalization

2.1.1 Material

- Polystyrene carboxylate microspheres (Polysciences)

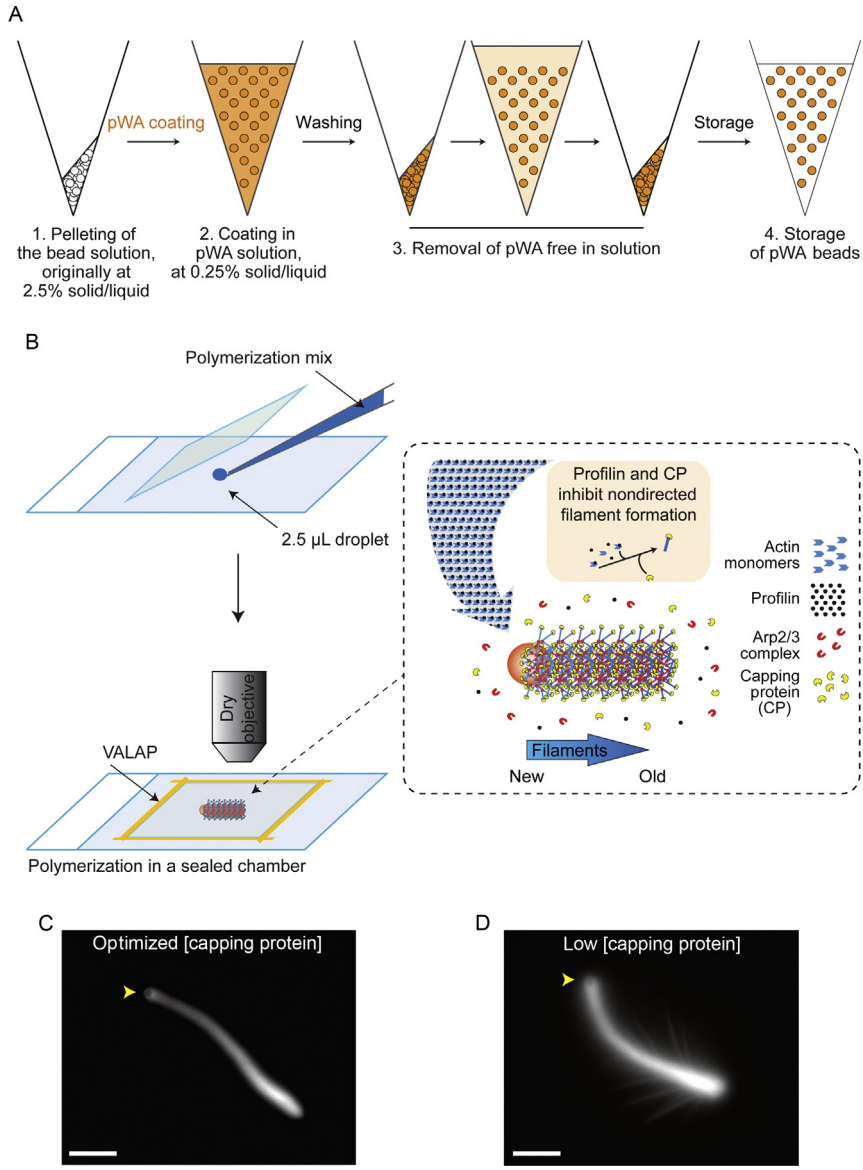

Figure 16.1 Actin-based motility in a G-actin buffered medium. (A) Schematic representation of the functionalization of polystyrene beads with pWA, an actin nucleation promoting factor. The crucial step of this procedure is the removal of pWA free in solution after the coating in order to prevent nondirected actin assembly in the medium. (B) The polymerization medium is placed between slide and coverslip in a sealed chamber, and bead motility is followed using epifluorescence microscopy. The polymerization medium contains a threefold excess of profilin (black) over actin (blue) in order

- BSA, Sigma A7030, resuspended in MilliQ water solution to make a 10% (w/v) solution and stored at −20 °C
- X buffer containing 10 m*M* HEPES (pH 7.5), 0.1 *M* KCl, 1 m*M* $MgCl_2$, 1 m*M* ATP, and 0.1 m*M* $CaCl_2$

2.1.2 Equipment

- Centrifuge
- Thermomixer (Eppendorf)

2.1.3 Methods

As illustrated in Fig. 16.1A, bead coating with NPFs is performed as follows:

1. Pellet 5 μL polystyrene carboxylated beads (16,000 × *g*, 2 min, room temperature).
2. Incubate beads pellet in usually 50 μL NPFs (900 rpm, 15 min, 20 °C in a thermomixer block, or even on a rotator at room temperature). Usually, we use 2 μ*M* pWA fragment of WASP protein, purified as described (Achard et al., 2010).
3. Pellet the NPFs-beads (16,000 × *g*, 2 min, 4 °C).
4. Carefully discard the supernatant. This step is crucial as the presence of free NPFs in solution will activate the Arp2/3 complex-mediated actin assembly and competes with polymerization on beads.
5. Incubate the functionalized NPFs-beads in 100–300 μL of 1% BSA in X buffer for at least 15 min on ice in order to saturate the space left free on beads surface and more importantly to get rid of free NPFs remaining in the pellet volume. Therefore, adjust the volume of BSA solution according of the adsorption efficiency of the NPFs to set the good balance between free NPFs removal and NPFs density on beads.
6. Centrifuge (16,000 × *g*, 2 min, 4 °C) and resuspend the bead pellet in 0.1% BSA in X buffer.
7. Store at 4 °C for up to 3 days.

---

to efficiently inhibit spontaneous actin nucleation in the medium, and the amount of capping protein (yellow) required for reconstituted motility blocks spontaneous nucleation coming from the small amount of actin monomers not bound to profilin. Actin nucleation and elongation is directed to pWA-coated beads through the recruitment and activation of the Arp2/3 complex (red). (C and D) Reconstituted actin-based motility of 2 μm beads in a medium containing 6 μ*M* actin monomers, 18 μ*M* profilin, 150 n*M* Arp2/3 complex, and 20 n*M* capping protein (C) or 10 n*M* capping protein (D). Scale bars are 10 μm.

2.2. The motility assay

2.2.1 Material

- Glasses and coverslips (Agar Scientific).
- G buffer containing 2 m*M* Tris–HCl (pH 7.5), 0.2 m*M* ATP, 0.5 m*M* DTT, 0.1 m*M* $CaCl_2$, 1 m*M* NaN_3.
- 10% BSA solution and X buffer as mentioned in the former section.
- 3 × Exchanging buffer: EGTA, 600 μ*M*, and $MgCl_2$ at three times (10 μ*M* + *C*) where *C* is the concentration of the actin solution to be Ca–Mg exchanged, and *C* is usually tens of micromolar.
- ATP solution containing 24 m*M* $MgCl_2$, 12 m*M* ATP, 20 m*M* DTT, 0.88 m*M*DABCO (1,4-diazabicyclo[2.2.2]octane solution from SIGMA).
- Methylcellulose, 1500 cPs (Sigma) resuspended in MilliQ water solution to make a 2% solution and stored at room temperature for a week.
- VALAP soft wax made of equal weights of Vaseline, Lanolin, and Paraffin wax (VWR). VALAP is maintained molten on heater block at 50–55 °C. The VALAP wax is a biologically inert material and therefore preferred to nail polish for coverslip sealing.

2.2.2 Equipment

- A dry block heater (VWR), in case of using VALAP to seal the motility chamber.
- Epifluorescence microscope. Images can be taken using dry 40 × objective, a motorized *XY* stage, and a CCD camera. The use of the motorized stage is useful as it allows acquiring actin dynamics on several beads under exactly the same biochemical conditions.

2.2.3 Methods

The following steps have to be performed in parallel:

(1) G-actin/profilin complex preparation

Extemporaneously prepare:

- Monomeric actin solution at a given *C* concentration (typically 3–6 μ*M*). According to the experiment's needs, the actin solution may contain nonlabeled or usually 5–10% Alexa labeled-actin.
- Mix the actin solution with a 1 × Exchanging buffer.
- Incubate for exactly 5 min on ice. At this step, the monomeric actin is Mg–ATP loaded.
- Add three times molar excess of profilin with respect to the final actin concentration.
- Incubate for at least 5 min on ice. At this step, actin monomers are mainly in the form of profilin–Mg–ATP–G-actin complex, ready to

be used. We recommend preparing the profilin/actin complex before every experiment.

(2) Motility medium

Prepare the following mix respecting the order and proportions:

- 2 μL of 10% BSA
- *x* μL Xb to make 15 μL in total
- 3 μL ATP mix
- 1 μL Arp2/3 complex to make 100–120 n*M* final
- 1 μL CP solution to make 20–30 n*M* final
- 0.5 μL NPFs-beads
- 2 μL of 2% methylcellulose
- *y* μL profilin–G-actin to make usually 1–4 μ*M* final
- Place 3 μL of the motility medium between glass and 20 × 20 coverslip (Fig. 16.1B)
- Check the onset of the reaction, seal with VALAP before evaporation
- Observe by phase contrast microscopy and/or by fluorescence microscopy (when using labeled proteins) (Fig. 16.1B). The presence of the singlet O_2 scavenger, DABCO, decreases the oxidative damage induced by photodynamic reactions

The bead motility assay is an extremely useful assay that allows the study of how biochemical parameters control actin network dynamics and architectural organization. We tested the role of CP in organizing the actin filaments into a network that is capable of propelling beads. By efficiently blocking barbed-end elongation, the CP protein restrains filament nucleation and elongation at the site of nucleation around the particle (Fig. 16.1B and C; Achard et al., 2010; Loisel et al., 1999). Therefore, decreasing the amount of CP in the medium leads to inefficient blocking of actin filament barbed ends initiated at the nucleating bead surface. Thus, actin filaments are able to elongate as the bead propulsion proceeds. This population of uncapped filaments gathers into bundles and consumes monomers but is only able to inefficiently produce bead propulsion (Fig. 16.1D; Pantaloni, Boujemaa, Didry, Gounon, & Carlier, 2000).

3. ASSEMBLY OF BRANCHED ACTIN NETWORKS ON A WIDE RANGE OF GEOMETRIES

Examination of actin network dynamics in living cells reveals how actin cytoskeleton structures and cell morphology are intimately related. During the past decades, a rich body of experimental work has revealed

how the cell's morphogenetic processes are powered by actin cytoskeleton dynamics (Fletcher & Mullins, 2010; Pollard & Borisy, 2003). However, conversely, little is known about how cell boundaries regulate the geometrical organization and the dynamics of the actin cytoskeleton. To improve our understanding of such questions, we have developed a UV-patterning procedure (Reymann et al., 2010, 2012) to study how nucleation geometries may regulate network dynamics and architecture. In the following section, we discuss how the UV-patterning method can be applied to study effect of different nucleation geometries on the assembly of branched actin networks, similar to those present at the leading edge of motile cells.

3.1. Design and functionalization of UV-patterned surfaces

UV-micropatterning method had been extensively described (Reymann, Guérin, Théry, Blanchoin, & Boujemaa-Paterski, 2014). Hereafter is a brief description of the passivation of glass coverslips with a poly(L-lysine)-poly (ethylene glycol), PLL-PEG layer (Fig. 16.2).

3.1.1 Material

- 20 × 20-mm glass coverslips and cover glasses (Agar Scientific)
- Ethanol, MilliQ water, Hellmanex III, isopropanol
- Parafilm
- PLL-PEG powder stored at −20 °C (JenKem Technology)
- PLL-PEG stock solution: 1 mg/mL PLL-PEG in Hepes 10 m*M* pH 7.4 (store at 4 °C for a week). Optimized coating with a regular layer of PLL-PEG chains depends on the efficiency of the plasma-cleaning procedure and the freshness of the PLL-PEG stock solution
- 10 × KMEI buffer containing 500 m*M* KCl, 10 m*M* $MgCl_2$, 10 m*M* EGTA, and 100 m*M* imidazole, pH 7.0
- 1 × KMEI prepared in G buffer (as in Section 1.1.2)
- Petri dishes (for storage of cleaned and passivated glass surfaces)

3.1.2 Equipment

- Plasma cleaner Femto (Diener electronic)
- UV ozone oven, UVO cleaner (Jelight)
- A chrome mask transparent to UV at the sites of micropatterns (TOPPAN, Photomask) and a vacuum mask holder, as described in Azioune, Storch, Bornens, Thery, and Piel (2009)

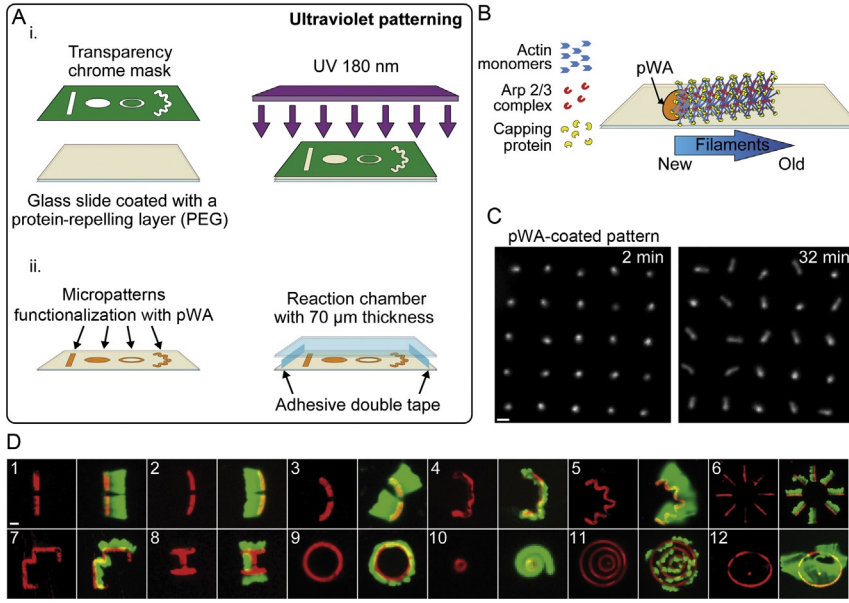

Figure 16.2 Reconstituted actin-based motility using UV patterning. (A) A chrome photomask containing transparent micropatterns is placed on a PLL-coated glass slide and exposed to ultraviolet light for 5 min (i). The micropatterned glass slide is incubated for 15 min with 1 μ*M* pWA prior to mounting in a reaction chamber (ii). (B) pWA-coated micropatterns are incubated with a motility medium containing actin monomers saturated with profilin (blue), Arp2/3 complex (red), and capping protein (yellow), resulting in the formation of actin filament networks. (C) Dot patterns (3 μm) are imaged by epifluorescence microscopy in a motility medium containing 6 μ*M* actin monomers (Alexa568 labeled), 18 μ*M* profilin, 150 n*M* Arp2/3 complex, and 25 n*M* capping protein. (D) Patterns with different geometries (red patterns, images from 1 to 12) are coated with pWA and fibrinogen 546 and then incubated with a mix containing 4 μ*M* actin monomers (Alexa488 labeled), 12 μ*M* profilin, 150 n*M* Arp2/3 complex, and 25 n*M* capping protein. The second image of the 12 pairs shows the actin network (green) developed after 1 h of polymerization. The width of each pattern line is 3 μm. Scale bars are 5 μm.

3.1.3 Methods

(1) Surface cleaning and PLL-PEG coating

In order to obtain a uniform layer of PLL-PEG, we first perform a drastic cleaning procedure that ensures a total removal of dusts and fats from the glass surfaces. Therefore, the washings in water are crucial as they allow removal of chemicals potentially harmful for proteins integrity and actin polymerization.

1. Slides are washed with 100% ethanol, wiped with absorbent paper, rinsed with MilliQ water, and then dried with a filtered airflow.
2. Slides are sonicated in acetone (30 min, room temperature), incubated in ethanol (10 min, room temperature), and then washed extensively with MilliQ water.
3. Slides are incubated in 2% Hellmanex (2 h, room temperature), washed extensively with MilliQ water, dried with a filtered airflow, and then stored at 4 °C in a clean box.
4. Cleaned slides are oxidized with O_2 plasma (3 min, 80–90 Watts).
5. Immediately after plasma oxidation, each coverslip is incubated with 100 μL of 0.1 mg/mL PLL-PEG solution on parafilm (30 min, room temperature). To gently lift up the coated coverslip, 100 μL of Hepes 10 m*M* (pH 7.4) is injected between glass and parafilm. If the coating was successful, the glass should come off dry, and the remaining tiny droplets at its edges can be wiped or blown off using pulsed air directed toward the noncoated side.
6. PLL-PEG-coated coverslips can be stored in Petri dishes at 4 °C for up to 2 weeks. The Petri dishes are sealed with parafilm to avoid desiccation.

(2) Surface patterning and functionalization

As previously described, we found that functionalization is the most efficient when performed immediately after UV insolation. As a control, patterns efficiently coated should initiate massive actin assembly within 5 min after the incubation with the polymerization medium detailed in the following section (Fig. 16.2A).

1. A chrome mask is washed successively with MilliQ water and isopropanol, dried with a filtered airflow.
2. The PLL-PEG coverslip is positioned on the vacuum mask holder facing upward, and the mask is placed on top of it. The vacuum as well as the absence of any dust ensures the tight contact between the coverslip and the mask, which is mandatory for obtaining reproducibly well-defined micropatterns.
3. After preheating the UV oven as recommended in the manufacturer's instructions, the PLL-PEG coated side of the coverslip is UV irradiated through the chrome mask for 5 min.
4. Immediately after UV patterning, each coverslip is incubated with 30 μL NPFs solution at a final concentration of 1–2 μ*M* (15 min on parafilm, room temperature). We usually use pWA fragment at 1 μ*M*. To remove the coverslip from the parafilm, 1 mL of

1 × KMEI buffer is injected between glass and parafilm. Each coverslip is then gently washed for 30 s in a small Petri dish containing cold 1 × KMEI. Functionalized coverslips must come off dry and the remaining droplet can be wiped or blown off using filtered-air flow directed toward the nontreated side.

5. Functionalized coverslips are stored for 48 h in a clean box at 4 °C.

3.2. Polymerization of branched actin filament network on UV-micropatterns

In order to study how geometry may control the actin dynamics and architectural organization of branched networks in a physiologically relevant medium, we polymerized dynamic actin network on micropatterned surfaces in the presence of the Arp2/3 complex and CP. CP is known to control filaments length and subsequently enhances branches density of Arp2/3-mediated networks (Blanchoin et al., 2000; Fig. 16.2B).

3.2.1 Material

- X buffer, 10 × KMEI buffer, G buffer, ATP mix, 10% BSA, 2% methylcellulose, VALAP, and freshly prepared profilin–Mg–ATP–actin (5–10% Alexa labeled), as in Section 1.1
- Adhesive double tape. We use a precut double tape 70 μm thick (LIMA)

3.2.2 Equipment

- 76 × 26 × 1.0-mm glass slides (Agar Scientific)
- A dry block heater (VWR) if using VALAP to seal the motility chamber
- Epifluorescence microscope, as described in Section 1.1

3.2.3 Methods

1. A flow cell chamber is freshly assembled as follows:
   - A glass slide is washed in water, wiped with ethanol and extensively rinsed with water just before use.
   - With a functionalized coverslip, a cleaned glass slide and precut adhesive double tapes assemble a stable flow chamber (Fig. 16.2A).
2. Immediately afterward, the motility medium, detailed in Section 1.1.2, is prepared in the same order and proportions excluding, however, the NPFs-coated beads.
3. Without delay, fill in the flow chamber with the motility medium.
4. Check the onset of the reaction and seal with VALAP before evaporation.

5. Follow assembly using fluorescence microscopy (Fig. 16.2 B, C, and D). Using this protocol, we were able to show that nucleation geometry can control the organization of branched networks. We polymerized these reticulated actin networks on a wide range of micropatterned nucleation geometries. The activation of the Arp2/3 complex and the recruitment of a preexisting filament at the pattern surface triggers branched actin filaments assembly. Since the CP blocks barbed-ends elongation, and the already assembled network serves as template for Arp2/3 nucleation activity at the pattern surface, the branched actin network grows off the pattern surface and adopts an organization consistent with the geometry of nucleation area (Fig. 16.2 B, C, and D).

4. RECONSTITUTION OF 3D CONNECTIONS OF STRUCTURED ACTIN NETWORKS

Combining the use of micropatterned geometries and the reconstituted motility assay performed in physiologically relevant medium, we were able to address two main questions. First, to what extent does geometry control dynamics and architecture of branched actin networks? Second, are we able to develop a new method based on actin filament self-organization to generate geometrically defined 3D connections of complex network organizations, which could exist *in vivo* or serve as a template for the engineering of bioinspired 3D systems? The following section explains how combining laser patterning and reconstituted biochemical media enables the control of such directed 3D connections of self-organized networks (Galland et al., 2013).

4.1. Design and functionalization of laser-patterned surfaces

Compared to UV-patterning, using lasers to pattern surfaces gives a significant advantage since it permits the high-precision positioning of motifs to be printed on two opposite walls of a preassembled chamber. This allows the precise direction of the interaction of networks growing off opposite patterns and the construction of 3D actin networks.

4.1.1 Material

- Coverslips (Agar Scientific)
- Adhesion promoter TI-Prime (MicroChemicals)
- 1% polystyrene (Sigma) in toluene (Sigma)
- 10× KMEI buffer, G buffer as in Section 1.1
- PLL-PEG stock solution as in Section 1.2
- Adhesive double tape. We use a precut double tape 30 μm thick (LIMA)

4.1.2 Equipment

- Spin coater WS-400-6NPP (Laurell technologies)
- Heating plate
- Oxygen plasma oven (FEMTO, Diener Electronics)
- Nanoablation station: inverted microscope (TE2000-E, Nikon) equipped with a CFI S-Fluor oil objective (100 ×, NA 1.3, Nikon), a perfect focus system (Nikon), motorized stage (Marzhauser), and a dual-axis galvanometer that focalizes the laser beam on the sample on the field of the camera, including a telescope that adjust the laser focalization with the image focalization, and polarizer to control the laser power (iLasPulse device, Roper Scientific). The microscope uses a pulsed laser passively Q-switched laser (STV-E, TeamPhotonics) that delivers 300 ps pulses at 355 nm (energy per pulse 1.2 μJ, peak power 4 kW, variable repetition rate 0.01–2 kHz, average power $\leq$ 2:4 mW). The laser was scanned throughout the region of interest with a power set to 300 nJ. The laser displacement, exposure time, and repetition time were controlled using Metamorph software (Universal Imaging Corporation).

The microscope is moreover equipped with a fluorescence illumination system X-Cite 120PC Q (Lumen Dynamics) and QuantEM:512SC camera (Photometrics) to monitor the laser printing procedure (for further details refers to Vignaud et al., 2012; Fig. 16.1A).

4.1.3 Methods

1. Prepare polystyrene-PLL-PEG-coated coverslips as follows. For a detailed protocol, refer to Azioune et al. (2009).
   a. Cleaned coverslips were spin-coated (30 s, 1000 rpm) with TI-Prime, backed on a heating plate (5 min, 120 °C), and then spin-coated with 1% polystyrene (1000 rpm, 30 s).
   b. Polystyrene-coated coverslips were oxidized with oxygen plasma (30 s, 60 W), and then incubated with 0.1 mg/mL PLL-PEG (30 min, room temperature; as in Section 1.2.1).
2. Assemble flow chamber using adhesive double tape and two polystyrene-PLL-PEG-coated coverslips with their treated sides facing inwards. Stably mount it on the motorized stage.
3. Define the regions of interest, ROI, to be laser printed.
4. Printing a pair of superimposed motifs is performed manually:
   a. Focus on the image on the interface glass/PLL-PEG layer. Little tiny particles of dust remaining on the glass help focalization (they however should be rare if glasses preparation was good).

b. The laser beam should be then similarly focused. However, for an efficient oxidation of the PEG chains, we slightly unfocus the laser setting the focal plane above the glass surface in order to hit the PEG layer.

c. Select a predefined ROI and laser print it. Each laser spot is exposed for 5 ms at a repetition rate of 2000 Hz.

d. Once completed, *without changing the* (x,y) *coordinates*, move on the z direction and repeat steps a and b on the upper coverslip.

e. Given the geometry of the ROI already printed and thanks to the precise move of the laser beam to adequate (x,y) coordinates using the software, it is easy to precisely control the position of the next motif to be printed in the opposite glass. For instance, the Metamorph software offers the function "move to relative position," which enables precise movement of the motorized stage and laser repositioning on the coverslip. For the upper coverslip, each spot was exposed for 8 ms at a repetition rate of 2000 Hz.

f. Select the predefined ROI and laser print it.

5. Repeat step 3 as many times as needed.

6. Instantly after completion of laser printing procedure, fill the flow cell with NPFs solution (15 min, room temperature). We use to coat with 1 μM pWA fragment of WASP protein.

7. Wash the flow cell with 1 × KMEI buffer and store at 4 °C for 2–3 days.

4.2. Assembly of 3D connections of structured actin networks

4.2.1 Material

- Solutions and extemporarily prepared motility medium as described in Section 1.2.2.

4.2.2 Equipment

- A dry block heater (VWR) if using VALAP to seal the motility chamber.
- Confocal microscope: Eclipse TI-E Nikon inverted microscope equipped with a CSUX1-A1 Yokogawa confocal head, an Evolve EMCCD camera (Roper Scientific), a CFI Plan APO VC oil objective (60 ×, NA 1.4) or a CFI Plan Fluor oil objective (40 ×, NA 1.3) (Nikon), and a motorized stage MS 2000 (ASI imaging). The system was driven by Metamorph software (Universal Imaging Corporation).

4.2.3 Methods

- Fill in freshly functionalized laser-patterned flow cell with the motility medium, detailed in Section 1.1.2, respecting preparation order and proportions but excluding NPFs-coated beads.

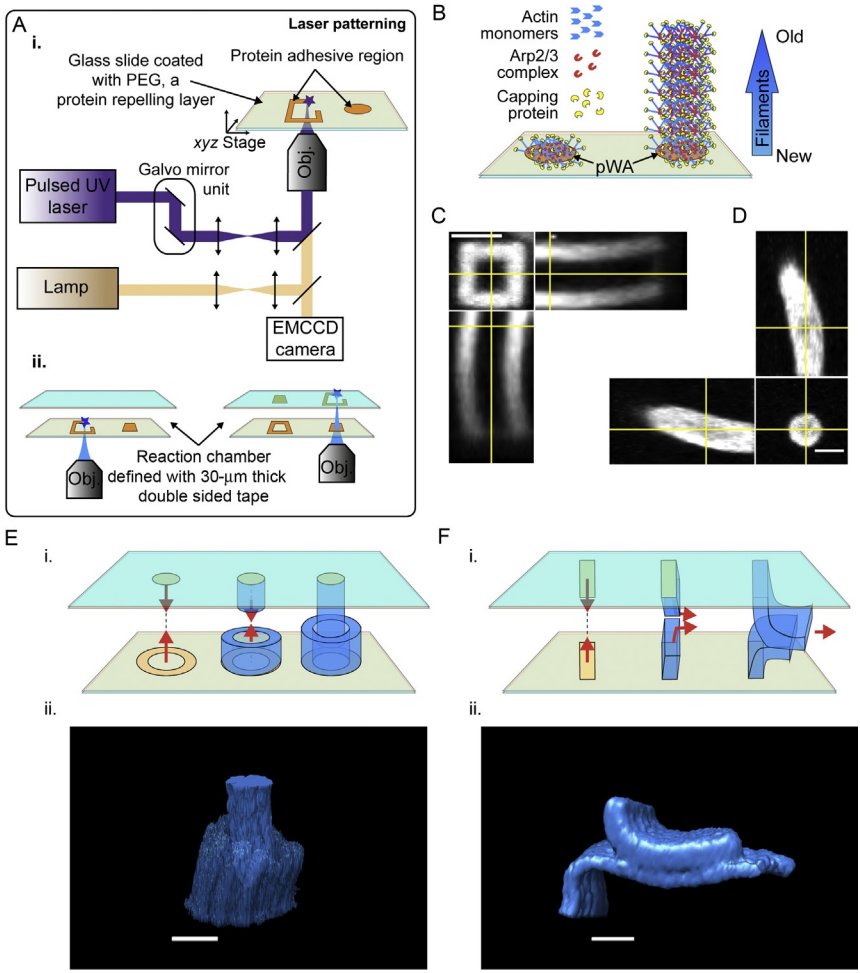

Figure 16.3 Laser patterning and oriented growth of actin structures in 3D. (A) Schematic representation of the laser-based patterning method. A pulsed UV laser is used to oxidize a protein-repellent layer of polyethylene glycol (PEG) to make it locally adhesive (i). Laser patterning of adhesive regions in a reaction chamber defined by two pegylated coverslips separated by 30–60 μm thick double-sided tape (ii). (B) Schematic representation of the growth of 3D actin structures from a nucleating pattern coated with the pWA in the presence of 3 μ*M* actin monomers (Alexa568 labeled), 9 μ*M* profilin, 50 n*M* Arp2/3 complex, and 60 n*M* capping protein. (C and D) 3D confocal images (planar, horizontal, and vertical cross sections) of actin structures polymerized from an empty square-shaped nucleating pattern (C) and from a disc-shaped nucleating pattern (D). (E) Schematic representation of the interaction of two actin structures growing face-to-face from two complementary-shaped nucleating patterns to form a 3D connection (i) and 3D reconstruction of confocal imaging of such a 3D connection (ii). (F) Schematic representation of the interaction of two actin structures growing face-to-face from two similar rectangular-shaped nucleating patterns that induce the formation of an actin structure in a plane parallel to the coverslip (i) and 3D reconstruction of confocal imaging of such a structure (ii). Scale bars are 10 μm.

- Check the onset of the reaction and seal the chamber with VALAP.
- Follow polymerization dynamics with a confocal microscope:
  - On each coverslip, in agreement with results with UV-patterned motifs, actin cross-linked structures grow normal to glass surface (Fig. 16.3B) and adopt the geometry of the pattern (Fig. 16.3C and D).
  - Judicious choice of pairs of patterns allows a fine control of the 3D connections between dynamic networks, which may lead to a "plug-and-socket-like connection" (Fig. 16.3E) or to "collision and release" connection (Fig. 16.3F).

5. CONCLUDING REMARKS

Investigations of the cell cytoskeleton reveal an extremely complex organization (Svitkina & Borisy, 1999; Xu, Babcock, & Zhuang, 2012). Specialized dynamic networks of a specific architecture and biochemical composition overlap and interconnect to build-up an entangled and reticulated web. The UV and laser-patterning procedures described here are valuable tools in deciphering how geometrical and biochemical constraints control the assembly of self-organized and dynamic actin structures. These reconstitution systems may pave the way for investigating the complex network interactions that occur *in vivo*. These methods are flexible and scalable, as one can biomimic more complex architectures using an unlimited variation of geometries, nucleation-promoting factors, or other regulatory proteins.

ACKNOWLEDGMENTS

This work was supported by grants from Human Frontier Science Program (HFSP RGP0004/2011 awarded to L. B.), Agence Nationale de la Recherche (ANR-08-BLANC-0012 awarded to L. B.), the "Chimtronique" programme of CEA to M. T. R. B. is a member of the Institut Universitaire de France. We thank Patrick Leduc and David Peyrade for insightful suggestions in building 3D connections and Chloé Zubieta for critical reading of the chapter.

REFERENCES

Achard, V., Martiel, J.-L., Michelot, A., Guérin, C., Reymann, A.-C., Blanchoin, L., et al. (2010). A "primer"-based mechanism underlies branched actin filament network formation and motility. *Current Biology*, *20*, 423–428.

Akin, O., & Mullins, R. D. (2008). Capping protein increases the rate of actin-based motility by promoting filament nucleation by the Arp2/3 complex. *Cell*, *133*, 841–851.

Azioune, A., Storch, M., Bornens, M., Thery, M., & Piel, M. (2009). Simple and rapid process for single cell micro-patterning. *Lab on a Chip*, *9*, 1640–1642.

Bernheim-Groswasser, A., Wiesner, S., Golsteyn, R. M., Carlier, M.-F., & Sykes, C. (2002). The dynamics of actin-based motility depend on surface parameters. *Nature*, *417*, 308–311.

Blanchoin, L., Amann, K. J., Higgs, H. N., Marchand, J. B., Kaiser, D. A., & Pollard, T. D. (2000). Direct observation of dendritic actin filament networks nucleated by Arp2/3 complex and WASP/Scar proteins. *Nature*, *404*, 1007–1011.

Blanchoin, L., Boujemaa-Paterski, R., Sykes, C., & Plastino, J. (2014). Actin dynamics, architecture and mechanics in cell motility. *Physiology Review*, *94*, 235–263.

Cameron, L. A., Footer, M. J., Van Oudenaarden, A., & Theriot, J. A. (1999). Motility of ActA protein-coated microspheres driven by actin polymerization. *Proceedings of the National Academy of Sciences of the United States of America*, *96*, 4908–4913.

Dayel, M. J., Akin, O., Landeryou, M., Risca, V., Mogilner, A., & Mullins, R. D. (2009). In silico reconstitution of actin-based symmetry breaking and motility. *PloS Biology*, *7*, 1000201.

Fletcher, D. A., & Mullins, R. D. (2010). Cell mechanics and the cytoskeleton. *Nature*, *463*(7280), 485–492.

Frishknecht, F., Moreau, V., Röttger, S., Gonfloni, S., Reckmann, I., Superti-Furga, G., et al. (1999). Actin-based motility of vaccinia virus mimics tyrosine kinase signalling. *Nature*, *401*, 926–929.

Galland, R., Leduc, P., Guerin, C., Peyrade, D., Blanchoin, L., & Thery, M. (2013). Fabrication of three-dimensional electrical connections by means of directed actin self organization. *Nature Materials*, *12*, 416–421.

Giardini, P. A., Fletcher, D. A., & Theriot, J. A. (2003). Compression forces generated by actin comet tails on lipid vesicles. *Proceedings of the National Academy of Sciences of the United States of America*, *100*, 6493–6498.

Iwasa, J. H., & Mullins, R. D. (2007). Spatial and temporal relationships between actin filament nucleation, capping, and disassembly. *Current Biology*, *17*, 395–406.

Kawska, A., Carvalho, K., Manzi, J., Boujemaa-Paterski, R., Blanchoin, L., Martiel, J. L., et al. (2012). How actin network dynamics control the onset of actin-based motility. *Proceedings of the National Academy of Sciences of the United States of America*, *109*, 14440–14445.

Loisel, T. P., Boujemaa, R., Pantaloni, D., & Carlier, M.-F. (1999). Reconstitution of actin-based motility of Listeria and Shigella using pure proteins. *Nature*, *67*(53), 613–616.

Mogilner, A., & Zhu, J. (2012). Cell polarity: Tension quenches the rear. *Current Biology*, *22*, R48–R51.

Pantaloni, D., Boujemaa, R., Didry, D., Gounon, P., & Carlier, M.-F. (2000). The Arp2/3 complex branches filament barbed ends: Functional antagonism with capping proteins. *Nature Cell Biology*, *2*, 385–391.

Pantaloni, D., & Carlier, M.-F. (1993). How profilin promotes actin filament assembly in the presence of thymosinß4. *Cell*, *75*, 1007–1014.

Pollard, T. D., Blanchoin, L., & Mullins, R. D. (2000). Molecular mechanisms controlling actin filament dynamics in nonmuscle cells. *Annual Review of Biophysics and Biomolecular Structure*, *29*, 545–576.

Pollard, T. D., & Borisy, G. G. (2003). Cellular motility driven by assembly and disassembly of actin filaments. *Cell*, *112*, 453–465.

Reymann, A.-C., Boujemaa-Paterski, R., Martiel, J.-L., Guérin, C., Cao, W., Chin, H. F., et al. (2012). Actin network architecture can determine myosin motor activity. *Science*, *336*, 1310–1314.

Reymann, A.-C., Guérin, C., Théry, M., Blanchoin, L., & Boujemaa-Paterski, R. (2014). Geometrical control of actin assembly and contractility. *Methods in Cell Biology*, *120*, 19–38.

Reymann, A.-C., Martiel, J.-L., Cambier, T., Blanchoin, L., Boujemaa-Paterski, R., & Théry, M. (2010). Nucleation geometry governs ordered actin networks structures. *Nature Materials*, *9*, 827–833.

Reymann, A.-C., Suarez, C., Guerin, C., Martiel, J.-L., Staiger, C. J., Blanchoin, L., et al. (2011). Turnover of branched actin filament networks by stochastic fragmentation with ADF/cofilin. *Molecular Biology of the Cell*, *22*, 2541–2550.

Romero, S., Le Clainche, C., Didry, D., Egile, C., Pantaloni, D., & Carlier, M.-F. (2004). Formin is a processive motor that requires profilin to accelerate actin assembly and associated ATP hydrolysis. *Cell*, *119*, 419–429.

Schafer, D., Jennings, P. B., & Cooper, J. A. (1996). Dynamics of capping protein and actin assembly in vitro: Uncapping barbed ends by polyphosphoinositides. *Journal of Cell Biology*, *135*, 169–179.

Svitkina, T. M., & Borisy, G. C. (1999). Arp2/3 complex and actin depolymerizing factor/cofilin in dendritic organization and treadmilling of actin filament array in lamellipodia. *Journal of Cell Biology*, *145*, 1009–1026.

Theriot, J. A., Rosenblatt, J., Portnoy, D. A., Goldschmidt-Clermont, P. J., & Mitchison, T. J. (1994). Involvement of profilin in the actin-based motility of L. monocytogenes in cells and in cell-free extracts. *Cell*, *76*, 505–517.

Vignaud, T., Galland, R., Tseng, Q., Blanchoin, L., Colombelli, J., & Théry, M. (2012). Reprogramming cell shape with laser nano-patterning. *Journal of Cell Science*, *125*, 2134–2140.

Vignjevic, D., Yarar, D., Welch, M. D., Peloquin, J., Svitkina, T., & Borisy, G. G. (2003). Formation of filopodia-like bundles in vitro from a dendritic network. *Journal of Cell Biology*, *160*, 951–962.

Xu, K., Babcock, H. P., & Zhuang, X. (2012). Dual-objective STORM reveals three-dimensional filament organization in the actin cytoskeleton. *Nature Methods*, *9*, 185–188.